Fibers and Polymers 2021, Vol.22, No.4, 1082-1098
DOI 10.1007/s12221-021-0578-9

ISSN 1229-9197 (print version)
ISSN 1875-0052 (electronic version)

Mechanical, Thermal and Thermomechanical Properties of Sponge Iron Slag filled Needle-Punched Nonwoven Jute Epoxy Hybrid Composites

Ankush Sharma[1], Mahavir Choudhary[1], Pankaj Agarwal[2], Shivam Joshi[1], S.K. Biswas[1], and Amar Patnaik[1]*

[1]*Mechanical Engineering Department, Malaviya National Institute of Technology, Jaipur 302017, India*
[2]*Mechanical Engineering Department, Amity University Rajasthan, Jaipur 303007, India*
(Received May 20, 2020; Revised June 21, 2020; Accepted June 26, 2020)

Abstract: In the present research work, the needle-punched nonwoven jute epoxy composites are fabricated by varying the weight percentages of sponge iron slag in vacuum assisted resin transfer molding technique. This study examines the physical, mechanical and thermomechanical properties (i.e., density, water absorption, tensile, flexural, inter-laminar shear strength, compression, impact, fracture toughness and dynamic mechanical analysis) of unfilled and 8 wt.%, 16 wt.% and 24 wt.% of sponge iron slag filled composites under controlled operating conditions. Moreover, it is shown that all the mechanical properties improved with the increased in sponge iron slag content except for tensile strength which increased only upto 16 wt.%. This study also attempted for the analysis of thermal conductivity of the unfilled and particulate filled composites in experimentally by hot disc method. This work also presents both existing empirical models and numerical simulation analysis to evaluate the thermal conductivity of the developed composites. The numerical simulation values of the thermal conductivity demonstrated good agreement with the experimental values. At the end, Cole-Cole plot is drawn between loss modulus and storage modulus to understand the nature of the proposed composites.

Keywords: Sponge iron slag, Jute fiber, Fracture toughness, Numerical simulation, Thermal conductivity

Introduction

In the present era, there is a need for advanced materials that have low impact on the environment and possess good strength. Therefore, eco-friendly materials derived from the natural sources forced to draw the attention of many researchers in the direction of green materials which can replace the synthetic fibers in fiber-reinforced polymer composites for industrial applications [1,2]. The use of natural fiber composites has increased from the last few years due to its biodegradability, low cost, high specific strength and stiffness characteristics [3]. Natural fiber-reinforced polymer composite has various applications in almost all engineering sectors [4]. Hence, jute fiber seems to be a popular fiber among all the natural reinforcement materials because it is relatively cheap, commercially available in the required from and like other natural fiber it offers many advantages such as biodegradable, moderate mechanical features which make it better alternative of synthesis fiber [5]. Gupta [6] investigated the dynamic mechanical properties of jute/epoxy composite by varying the fiber loading from 10 to 40 wt.% prepared by hand-layup technique at 1, 2, 5 and 10 Hz frequency. Results concluded that the variation in frequency has a noteworthy effect on the DMA of the fabricated composites and load-bearing capacity is directly proportional to the fiber loading. The dynamic mechanical characteristics of the hybrid composite were prepared by varying the different percentages of jute and sisal fiber. It was observed that 50-50 wt.% of Jute and sisal fiber composite (J50S50) depicts excellent fiber-matrix adhesion [5]. Mechanical characterization of three different types of natural fiber (jute, hemp and flax) composite has been studied by Chaudhary *et al*. [7]. Improved tensile strength (58.59 MPa) were attained by hybrid composite (jute, flax and hemp epoxy composite) whereas jute, hemp-epoxy composites reported enhanced in flexural strength (86.6 MPa).

Regardless of numerous benefits, natural fibers have higher water absorption ability because of its hydrophilic nature which results in poor interfacial bonding and ultimately the properties composite was decreased [8,9]. The surface treatment processes of the natural fiber, such as alkaline, and silane treatment as per literature increased the interference bonding as well as decreased the water sorption competence [10]. Karabulut *et al.* [11] have studied the effect of surface modification with 5, 10 and 15 wt.% alkali solution on woven jute laminate composites. The modification process and matrix materials were significantly affect the mechanical properties of the jute laminate composites. Effect of surface treatment using sodium hydroxide (NaOH) and Maleic anhydride-grafted polypropylene (MPP) on the mechanical properties of the jute fiber/PP composite was studied by Liu and Dai [10]. They observed that the treatment of the fiber helps in to improve the mechanical properties of the composite significantly. Among all these treatment process, alkali treatment by using sodium hydroxide aqueous solution was effective and easy [12].

The addition of filler in the natural fiber reinforced polymer composite was considered to improve the physical and mechanical properties of the hybrid composites [13-15]. Various studies have shown the significant effect of filler on the physical, mechanical, thermal and thermomechanical

*Corresponding author: apatnaik.mech@mnit.ac.in

properties of the natural fiber reinforced polymer composites. Number of organic and inorganic filler materials like red mud, granite powder, marble dust, cement by-pass dust (CBPD), blast furnace slag, Al_2O_3, SiC, graphite, AlN etc. have been widely explored till date [13,15,17-22]. It has been observed that solid waste produced in significant quantity due to rapid industrialization is the main challenge associate with the environment pollution. Some industrial and stone wastes like blast furnace slag, CBPD, copper slag, red mud, granite dust and marble dust has already been practiced in the past research as a replacement of conventional metal and ceramic fillers in fiber reinforced polymer composites. In this view, sponge iron slag could be a potential filler material in order to improve the mechanical and thermomechanical properties. Pawar *et al*. [15] observed decrement in the tensile and flexural strength whereas, significant improvement in the fracture toughness with the increased in the granite powder as a filler in the jute fiber reinforced epoxy composite as fabricated by hand layup technique. Composite with 16 wt.% granite powder shows better viscoelastic properties compared to other developed composites. Sharma and Patnaik [13] developed marble dust filled needle punched jute/epoxy composite using vacuum assisted resin transfer molding technique (VARTM). The research was investigated the effect of marble dust loading in the resulting composite's mechanical and thermal properties and concluded that the loading of the marble dust up to 30 wt.% increased the flexural as well as interlaminar shear strength whereas, tensile strength was gradually decreased. Patnaik and Nayak [23] proposed that mechanical properties of the needle punched jute-epoxy composite increases with the increased in silicon carbide content from 0 to 15 wt.% whereas, the thermal conductivity of the same starts decreasing in nature. The same group again reported that at 15 wt.% silicon carbide addition the particulate filled composite shows improved in storage and loss modulus trend at higher temperature (upto 68 ^oC).

The thermal conductivity of the polymer composite depends upon multiple numbers of factors such as filler type, fiber orientation, filler shape and size, particle distribution, reinforced material in the composite. There are various methods for enhancing the thermal conductivity of the composite such as inclusion of conductive fillers, chemically treated fillers, etc. [19,24]. A lot of experimental as well as numerical and empirical studies have been done to predict the conductivity of the composite with and without incorporation of particulates [13,25,26]. The literature cites different types of two-phase empirical models to predict the effective thermal conductivity of the polymer composite but limited number of three-phase models has been introduced [27-29]. Besides experimental and analytical studies finite element (FE) simulation model have been a popular tool for the prediction of thermal conductivity. FE based thermal conductivity analysis of randomly oriented glass fiber composites was done by Patnaik *et al*. [30] and found number of divisions affecting the thermal conductivity of the composites. Kaundal *et al*. [19] performed finite element analysis to predict the thermal conductivity of SiC filled glass fiber composites and then compared with the experimental values. They observed that the predicted values were in the good agreement with the experimental one. Experimental and theoretical thermal conductivity of silicon rubber and Al_2O_3 particle based composite has been investigated by Gao *et al*. [31]. The thermal conductivity was increased with the increase in the volume fraction of the particle in the composite. A very few works have been reported on the measurement of thermal conductivity using finite element approach for particulate filled natural fiber reinforced polymer composite.

In current research work, micro sized sponge iron slag powder filled hybrid composite is prepared by varying the weight percentage of the filler from 0 to 24 wt.% at an interval of 8 wt.%. The physical properties (density), water absorption, mechanical characteristics (tensile strength, flexural strength, interlaminar shear strength (ILSS), compressive strength, impact energy and fracture toughness), thermal conductivity and dynamic mechanical characteristics (storage and loss modulus, damping factor, glass transitions temperature and homogeneity) are investigated. After analysis of the mechanical properties the fractured surfaces are then examined to understand the failure mechanism of the composite with the help of scanning electron microscopy. At the end, the obtained experimental thermal conductivity values of the composites are compared with both numerical as well as existing empirical models for validation purposes.

Experimental

Materials

Needle punched nonwoven jute fiber with areal density of 300 gsm (thermal conductivity=0.07 W/m-K, specific heat= 324 J/kg^oC) as shown in Figure 1(a) is employed as the reinforcing material purchased from Eskay International, Kolkata, India. CY230 (Epoxy) and HY951 (hardener) are

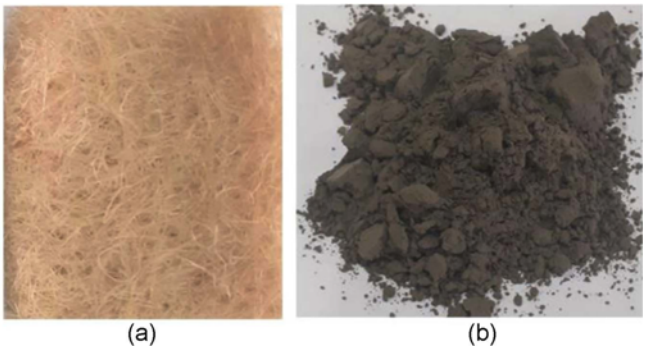

Figure 1. (a) Needle-punched nonwoven jute fiber and (b) sponge iron slag (SIS) powder.

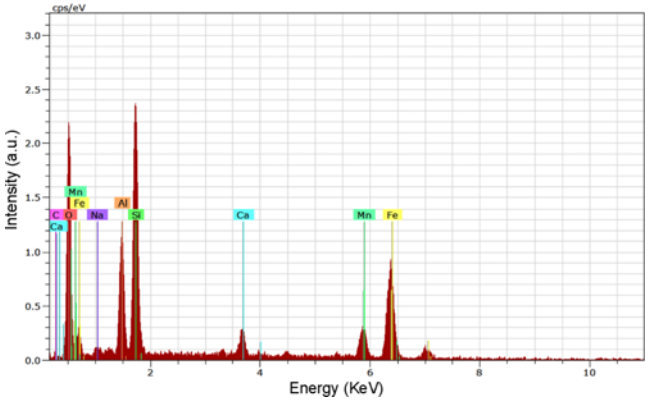

Figure 2. Energy-dispersive X-ray spectroscopy (EDS) analysis of SIS powder.

used as matrix material (thermal conductivity=0.268 W/m-K, specific heat=1000 J/kg°C) in the present work and procured from Excellence resin, Meerut, India. Filler material as SIS powder (thermal conductivity=2.13 W/m-K, specific heat=850 J/kg°C) as shown in Figure 1(b) is collected from the local sponge iron industry in the lumps form and then converted in the fine powder using ball mill (average size 10 μm). The SIS powder composed of mixture of oxides such as Fe_2O_3, SiO_2, Al_2O_3 and MnO respectively as depicted from the Energy-dispersive X-ray spectroscopy (EDS) (Figure 2). Other chemical elements such as Ca, C, Na are also present in the powder as shown in Table 1.

Alkaline Treatment

The needle-punched nonwoven jute fiber mats are soaked

Table 1. EDS results of SIS powder

Element	O	Fe	Si	Al	Mn	Ca	C	Na
wt.%	41.13	19.29	16.5	9.61	4.75	4.09	2.82	1.78
Atomic wt.%	58.94	7.92	13.5	8.17	1.98	2.34	5.38	1.77

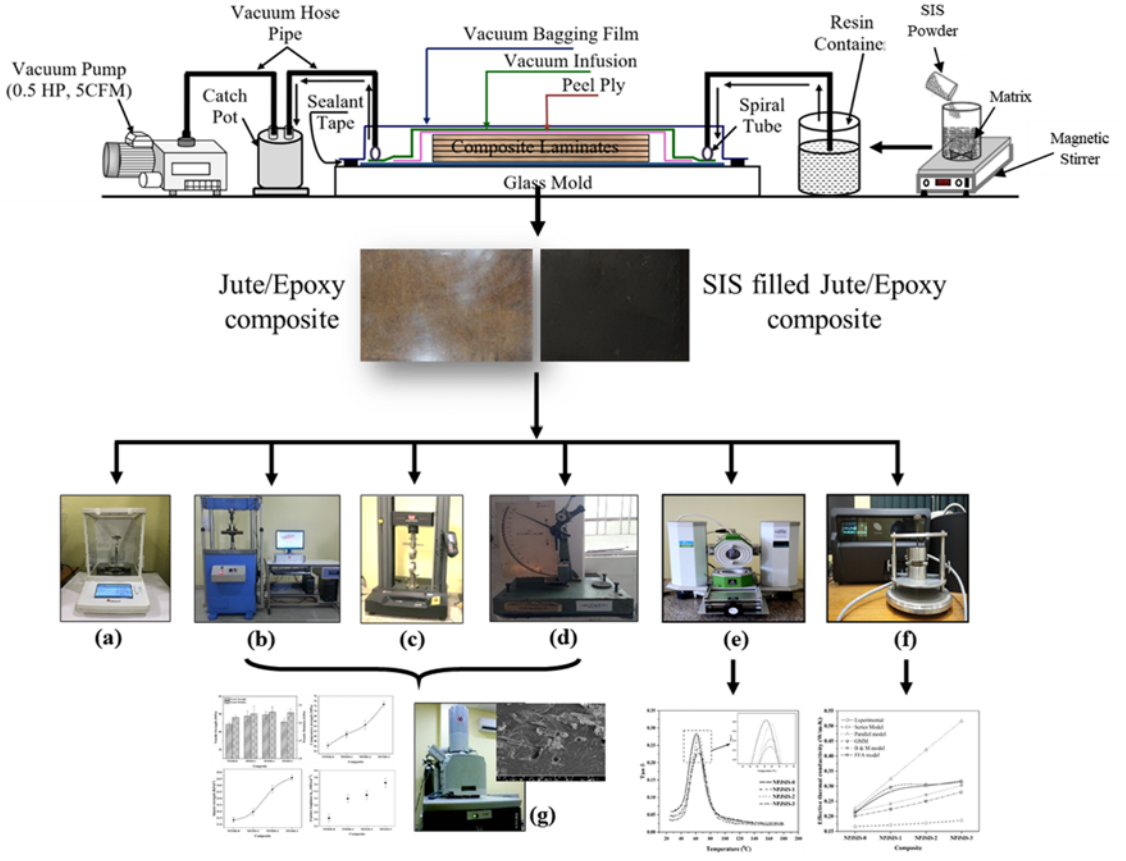

Figure 3. Schematic of composite fabrication process (VARTM) and its characterization; (a) density measurement, (b) Heico universal testing machine, (c) Instron 5967, universal testing machine, (d) impact testing machine, (e) dynamic mechanical analyser, (f) thermal conductivity measurement (TPS 500), and (g) SEM.

into a 5 % (w/w) aqueous NaOH solution for 2 hours and then rinsed with water multiple times to ensure the removal of NaOH adhering to the surface. Thereafter, fiber mats are dried in an oven at 60 ^{o}C for 10 hours.

Fabrication Technique

SIS powder is mixed in the matrix material with the help of magnetic stirrer at 800 rpm for 2 hours, followed by sonication at 50 Hz for 1 hr to ensure proper dispersion of the filler particles in the matrix material. The composite is then fabricated by varying the weight percentage of the SIS in the matrix from 0 to 24 wt.%, in the interval of 8 wt.%. VARTM process is adopted for the fabrication of the composites. Figure 3 describes the illustration of the experimental set up with details of processing constituents [13,14,32-34]. A layer of mold release agent (polyvinyl alcohol (PVA)) is initially sprayed on the surface of the glass mold. Thereafter, four layers of alkali treated jute fiber mats are stacked on the mold surface followed by peel ply and flowing media (infusion mesh). All the layers are covered by a flexible polymer mould to create vacuum environment. A flexible polymer bag is placed around the stack and sealed by a sealant tap. Later, the complete system is tested for 30 minutes to check the presence of any air intake. After confirmation of the complete leak-proof system, the matrix material is injected in the preform via plastic tubes by the combined action of gravity and vacuum pressure into the vacuum bag. The infusion process is terminated once complete impregnation is confirmed. After that, the impregnated layers are cured at room temperature for 24 hours. The developed composited with 0 wt.% (unfilled), 8 wt.%, 16 wt.% and 24 wt.% of SIS powder are designated as NPJSIS-0, NPJSIS-1, NPJSIS-2 and NPJSIS-3, respectively.

Density and Void Content

The experimental density of the unfilled and SIS powder filled needle-punched nonwoven jute/epoxy (NPJE) composites are measured using Archimedes principle as per ASTM standard using density measurement equipment (Radwag, AS 220. R2) whereas, the theoretical density is calculated by using rule of mixture technique. The percentage of void content in each fabricated composite are evaluated by comparing the experimental density with theoretical density [35].

Water Absorption and Kinetic Parameter

The water absorption test is conducted as per ASTM D5229 standard. Initially the weight of the test coupons is measured using electronic weighing machine (Radwag, AS 220. R2) with an accuracy of ±0.1 mg. All the samples are then immersed in the distilled water at room temperature. After the pre-decided immersion period the samples are taken out and wiped using tissue paper to remove the surface moisture. Immediately the samples are weighed to measure the mass gain if any. The procedure is repeated for each test. The percentage of water absorption after every test is calculated as per equation (1)

$$W_t(\%) = \left(\frac{W_f - W_i}{W_i}\right) \times 100 \tag{1}$$

where, W is the mass of the specimen and suffix t, f and i represents the total final and initial.

The kinetic parameter i.e., the Diffusion coefficient ($K_{coeff.}$) is measured from the slope (θ) of the water absorption against the time curve and calculated using equation (2) [5].

$$K_{coeff.} = \pi\left(\frac{x^2\theta^2}{16W_\infty^2}\right) \tag{2}$$

where, x, θ and W_∞ represents the initial sample thickness, slope of liner portion of water absorption curve and water absorption at infinite time.

Mechanical Characterization

ASTM D3039, ASTM D790 and ASTM D2344 standards are used to prepare the test specimens and perform the tensile test, flexural test and ILSS respectively. The experiments are conducted using a Universal testing machine (Make: Heico, India, Capacity 30 kN) with a crosshead speed of 1 mm/min for tensile test and 1.5 mm/min for three-point bending flexural strength and ILSS respectively. Three samples are tested in each test run and finally the average value is reported for further analysis.

Compression test is performed as per ASTMD3410 using universal testing machine (Make: Instron, US, Model: Instron 5967, Capacity 30 kN) with crosshead speed of 1.5 mm/min three samples of each composites is tested. The impact energy of the fabricated composite is measured by performing Izod impact test on impact testing machine as per ASTM D 256 standard. The three specimens of each composite are tested and average value is reported in all the above analysis for testing of mechanical analysis.

The plain strain fracture toughness (K_{Ic}: critical stress intensity factor) of the fabricated composite is evaluated in accordance with ASTM D5045-14 with single edge notch bending (SENB) specimen (Figure 4) using Universal testing machine (Make: Heico, India, Capacity 30 kN) with a crosshead speed of 1 mm/min under displacement mode. The pre-notch is formed using saw and then a pre-crack of around 1 mm is introduced using fine razor with constant ratio of crack length to width (φ) is between 0.45 to 0.55. The value of K_{Ic} (MPa·m$^{1/2}$) is evaluated by using equation (3) as follows:

$$K_{IC} = \frac{P_Q}{B\sqrt{W}} \times f(\varphi)$$

$$f(\varphi) = 6\sqrt{\varphi}\frac{[1.99 - \varphi(1-\varphi)(2.15 - 3.93\varphi + 2.7\varphi^2)]}{(1+2\varphi)(1-\varphi)^{1.5}},$$

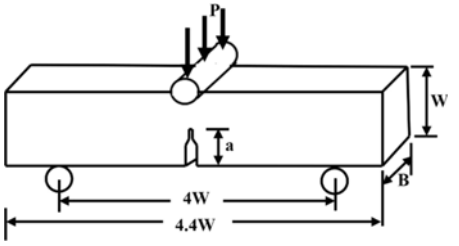

Figure 4. Schematic of SENB specimen as per ASTM 5045-14.

$$\varphi = \frac{a}{W} \tag{3}$$

where, P_Q: load (KN), B: sample thickness (cm), W: sample width (cm), a: crack length

The value obtained as per above described method are considered to be validated, once the following criteria are satisfied:

$$B, a, (W-a) > 2.5\left(\frac{K_Q}{\sigma_y}\right)^2 \tag{4}$$

where, K_Q and σ_y are the conditional K_{Ic} and material yield stress respectively.

Thermal and Thermomechanical Characterization

Thermal Conductivity

The thermal conductivity of the developed composites is experimentally measured using thermal constants analyser (Make: Hot Disk, Model: TPS 500). The thermal conductivity is measured based on the transient plane source. A Hot Disk sensor is placed between the two identical composite samples with a cross section of 25 mm×25 mm by keeping all other sides of the samples thermally insulated. Upon initialization, the electric current tends to flow in the hot disc sensor and the resistance is then measured as a function of time and the thermal conductivity is measured by monitoring the time temperature relationship at room temperature. The thermal conductivity of the developed composites are also estimated using existing theoretical relationships i.e., series model, parallel model, geometric mean model (GMM) and Brailsford and Major (B & M) model and well described in depth in numerous literature [19,30,36-39].

The parallel model and series models are described as per equations (5) and (6) [19]:

$$\gamma_c = \vartheta_f \gamma_f + \vartheta_m \gamma_m + \vartheta_p \gamma_p \tag{5}$$

$$\frac{1}{\gamma_c} = \frac{\vartheta_f}{\gamma_f} + \frac{\vartheta_m}{\gamma_m} + \frac{\vartheta_p}{\gamma_p} \tag{6}$$

where, γ, ϑ are the thermal conductivity and volume fraction and c, f, m, and p shows the composite, fiber, matrix and particulate respectively.

In the case of a geometric mean model (GMM) the effective thermal conductivity of the composite is given by equation (7) [19].

$$\gamma_c = \gamma_f^{\vartheta_f} \gamma_m^{\vartheta_m} \gamma_p^{\vartheta_p} \tag{7}$$

The two component models were expanded by Brailsford and Major (B & M) [27] to take account of single-disperse homogeneous particles made of two distinct materials randomly separated into a continuous matrix and the effective thermal conductivity is given by equation (8).

$$\gamma_c = \frac{\left\{\gamma_m \vartheta_m + \gamma_f \vartheta_f \frac{3\gamma_m}{(2\gamma_m+\gamma_f)} + \gamma_p \vartheta_p \frac{3\gamma_m}{(2\gamma_m+\gamma_p)}\right\}}{\left\{\vartheta_m + \vartheta_f \frac{3\gamma_m}{(2\gamma_m+\gamma_f)} + \vartheta_p \frac{3\gamma_m}{(2\gamma_m+\gamma_p)}\right\}} \tag{8}$$

Numerical Simulation Model and Assumptions

Finite element method is one of the strongest numerical tools for analysing transient thermal problems to solve the scientific problems with assumptions are to be considered in modelling and assigning the physical properties. The effective thermal conductivity is simulated using ANSYS tool and following assumptions are made for unfilled and SIS filled NPJE composites [40,41]:

a) The microstructure of unfilled and SIS powder filled NPJE composites are designed by taking the volume fraction of the unit cell.

b) No interfacial thermal resistance exists between SIS particles and matrix that means perfect bonding between the two solids.

c) Isotropic thermal conductivity, specific heat and density of SIS powder, Jute fiber and Epoxy matrix are selected.

Since the experimental sample size is large and in order to simulate the effect of filler loading on thermal conductivity a unit cell of 100×100 μm is considered as a control volume.

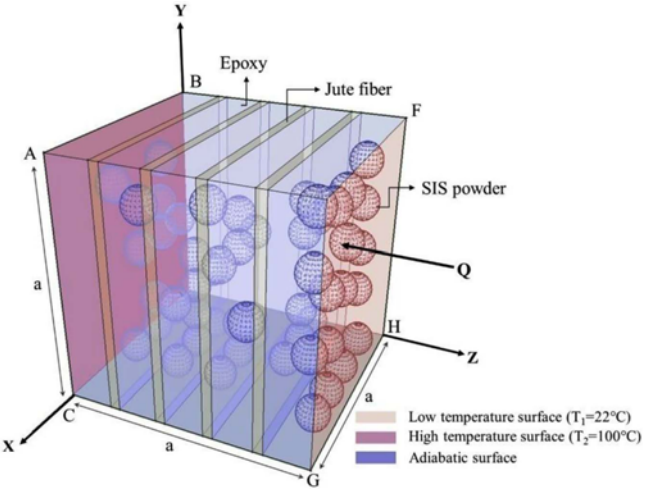

Figure 5. Boundary conditions for developed model.

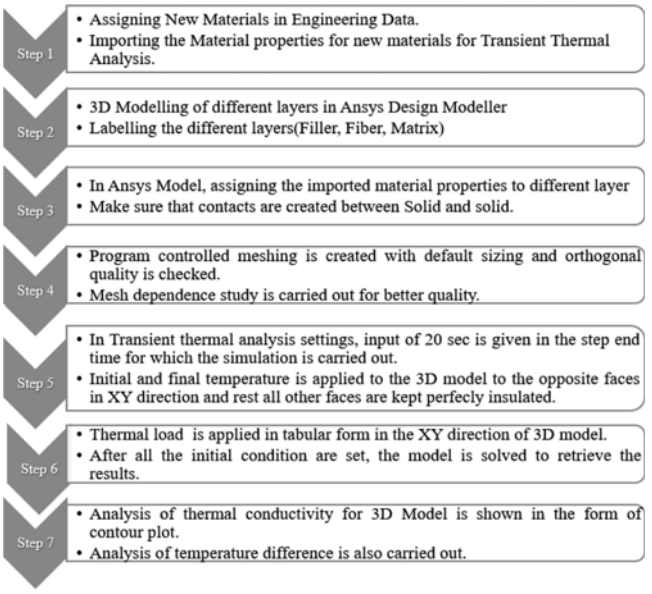

Figure 6. Steps for transient thermal analysis.

Figure 5 shows the numerical model and boundary conditions applied during analysis of the composites. Four layer of jute fiber (in vol.%) and five layer of matrix material (in vol.%) is considered. The filler particles are represented spherical in nature and randomly distributed as per filler vol.% in to each layer of the matrix. Three-phase models are generated by defining a particulate thermal conductivity values in the finite element model with number of elements distributed randomly within the matrix. In order to quantify the constitutive property of the composite, numerical model is applied instead of analytical approach due to the geometry complexity and the steps followed to perform the finite element simulation are shown in Figure 6.

The geometrical models of unfilled and SIS powder filled NPJE composites are generated in design modeller as shown in Figure 7(a and b). Due to the irregularity in model, it is discretized into the 4 node tetrahedron element for the further numerical solution using FEM and mesh refinement study is done on the particle element to ensure the convergence of thermal conductivity. The mesh refinement operation can split one particle element into multiple elements; therefore, those nodal values of the particle elements can provide greater precision when the properties of the particle elements differ significantly from those of the matrix elements. Based on the mesh refinement study, first order mesh is performed for the finite element analysis as depicted in Figure 8 and time integration method is used to perform transient thermal analysis followed by generalized trapezoidal rule. For the accuracy and stability of the solution, time step size of 80 sec is selected according to the Biot number and Fourier Number which depends on average elemental width, average density and specific heat respectively. Heat flow (0.1 W) with respect to time t (80 sec) along with initial temperature on the two opposite faces (T_1=22 °C and T_2=100 °C) are applied along z-direction and the remaining faces are set to be adiabatic as shown in Figure 5. The system is then solved by THOPT APDL command in transient thermal analysis.

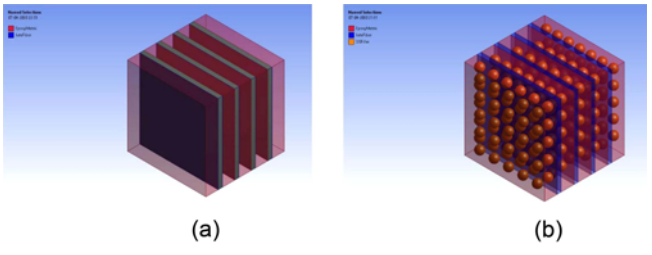

Figure 7. 3D geometry model for (a) unfilled NPJE composite and (b) SIS powder filled NPJE composite.

The governing equation for transient state heat conduction for 3-Dimensional cartesian coordinate system is given by [42,43]:

$$\frac{\partial}{\partial x}\left(\gamma_x \frac{\partial T_{(x,y,z,t)}}{\partial x}\right)+\frac{\partial}{\partial y}\left(\gamma_y \frac{\partial T_{(x,y,z,t)}}{\partial y}\right)+\frac{\partial}{\partial z}\left(\gamma_z \frac{\partial T_{(x,y,z,t)}}{\partial z}\right)$$
$$+Q_{(x,y,z,t)}=\rho C_p \frac{\partial T_{(x,y,z,t)}}{\partial z} \quad (9)$$

where, ρ, C_p, and Q denotes density and specific heat, and heat generated by the solid whereas subscript x, y, z and t shows thermal conductivity in x, y and z direction and time.

Since the differential equation equation (9) is of second order, at least two boundary conditions and one initial condition are required for the solution.

$$T_{(x,y,z,t)}=T_{0(x,y,z)} \text{ for } t>0 \text{ on } S_1 \quad (10)$$

$$\gamma_x \cdot \frac{\partial T}{\partial x} \cdot l_x+\gamma_y \cdot \frac{\partial T}{\partial x} \cdot l_y+\gamma_z \cdot \frac{\partial T}{\partial x} \cdot l_z+q=0$$
$$\text{for } t>0 \text{ on } S_2 \quad (11)$$

where, q is the heat flux, T_0 is the surrounding temperature, l_x, l_y, l_z are unit vector normal to the boundary, S_1 is the boundary (Dirichlet Condition) on which the value of the temperature is specified as $T_0(t)$, S_2 is the boundary (Neumann condition) on which the heat flux q is specified,

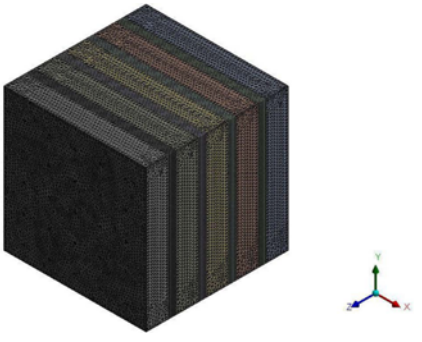

Figure 8. Meshing for NPJE composite.

and the initial Condition

$$T_{(x,y,z,t)}\big|_{t=0} = T_{0(x,y,z)} \tag{12}$$

Equation (12) is defined as initial condition at time zero as equation (9) is of first order differential equation in time t and finally, the thermal conductivity is calculated using Fourier's law

$$q = k\frac{dt}{dx} \tag{13}$$

Dynamic Mechanical Analysis

The viscoelastic characteristics of the composites are studied using dynamic mechanical analyser (Make: Perkin Elmer, Model: DMA 8000) confirming to ASTM D4065. The dynamic mechanical properties are evaluated in three-point bending mode with 1 Hz frequency as a function of temperature. The tests are carried out in the temperature range of 25 to 180 ^{o}C at a heating rate of 2 ^{o}C/min. The storage modulus, loss modulus, glass transition temperature and damping factor is measured.

Results and Discussion

Effect of SIS filler Loading on Density and Void Fraction

The physical and mechanical characteristics of the fiber reinforced polymer composite are significantly influenced by the voids present in the composite. The theoretical density always surpassed the measured densities and the difference between two represents the void content in the developed composites. The theoretical and measured densities in conjunction with corresponding void fraction of the fabricated composites are shown in Table 2.

The density of unfilled composites is 1.2248 g/cm^3 which increased to 1.2545 g/cm^3 by inclusion of 8 wt.% of SIS powder. The density of the fabricated composite progressively increases with the inclusion of SIS powder from 8 wt.% to 24 wt.% which is attributed to the higher density of SIS powder. It is clearly seen from Table 2 that void fraction of the fabricated composites are increased by 0.79 %, 1.41 %, 1.95 % and 2.15 % respectively with the increased in the filler from 0 wt.% to 24 wt.%. This may be attributed to the fact that addition of filler in the epoxy imparts resistance to the flow, thereby modifying the impregnation and curing characteristics of the matrix [44]. Also, the increase in void fraction in the composite is possible due to the air entrapped at the fiber, filler and matrix interface during impingement process [18]. Similar, trend were also observed by past researchers as reported in the cited references [13,15,45].

Table 2. Density and void volume fraction of manufactured composites

Composite	Theoretical density (g/cm^3)	Measured density (g/cm^3)	Void volume fraction (%)
NPJSIS-0	1.2248	1.2152	0.79
NPJSIS1	1.2545	1.2368	1.41
NPJSIS2	1.2824	1.2574	1.95
NPJSIS3	1.3093	1.2812	2.15

Effect of SIS filler Loading on Water Absorption Behaviour and Diffusion Kinetics

Water absorption test is conducted to measure the amount of water absorbed by the developed composites under specific conditions. The water absorption in a composite depends upon the number of factors such as fiber volume fraction, void content, temperature, humidity, viscosity of matrix etc. [46]. The water absorption of unfilled and SIS filled needle jute/epoxy composite is plotted against immersion time as shown in Figure 9. The water absorption percentage for all these composites are increased with the increase in immersion time and attains a saturation state at 3.37 %, 4.87 %, 5.49 % and 7.02 % for NPJSIS-0, NPJSIS-1, NPJSIS-2 and NPJSIS-3 respectively. The water absorption of the composite shows proportional behaviour with respect to the immersion time, filler content and void content. It is observed from Figure 9 that the water absorption is increased with an increased in SIS powder wt.% in the composites which is attributed to the presence of voids and hydrophilic nature of the jute fiber [5,47]. The water absorption of unfilled composite (NPJSIS-0) is indicated lower water absorption compared to SIS powder filled composites. It is also observed from the figure that initially the water absorption of the composites show liner nature and follows Fick's law of diffusion, the absorption is then nearly depleted and ultimately finished [48]. Figure 10 shows the diffusivity vs. fabricated composites. It is revealed

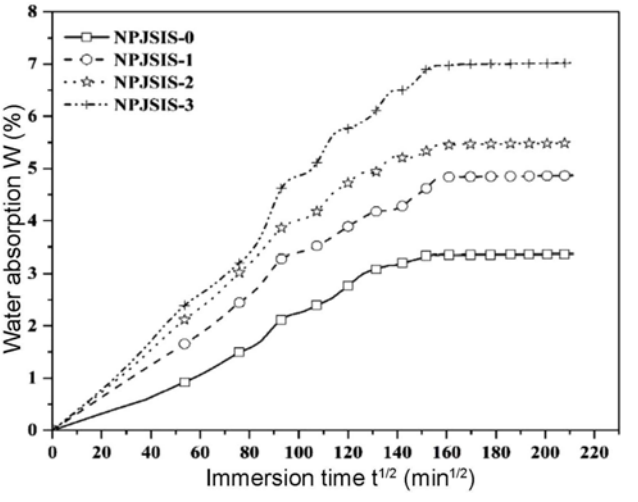

Figure 9. Water absorption of manufactured composites as a function of time.

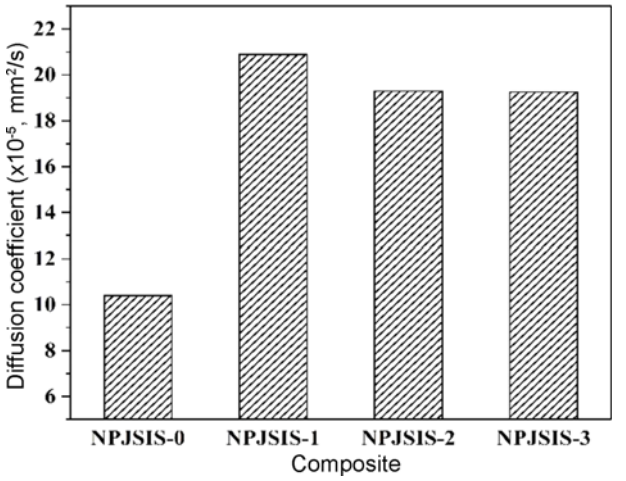

Figure 10. Diffusion coefficient curve for manufactured composite.

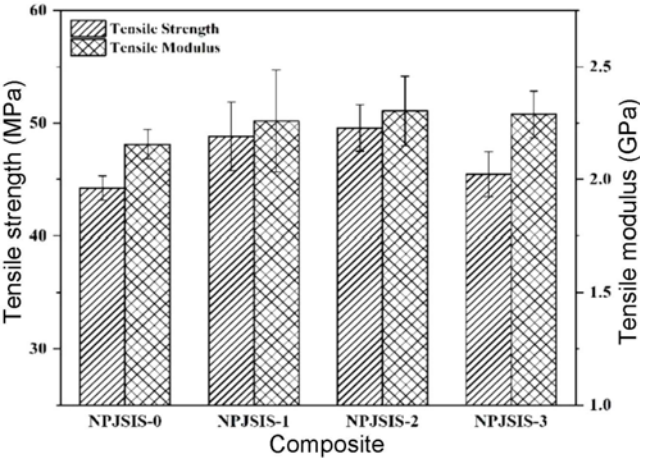

Figure 11. Tensile strength and tensile modulus of manufactured composite.

from the figure that the diffusion coefficient for NPJSIS-0 and NPJSIS-1 is 10.38×10^{-5} mm^2/s and 20.88 mm^2/s respectively, further increased in wt.% of SIS powder the diffusivity of the composite decreases and observed that the diffusion coefficient for NPJSIS-2 and NPJSIS-3 is dropped by 7.65 % and 7.76 % respectively compared with NPSIS-1. The reduction in the diffusion factor may be attributed to the strong adhesion between the fiber and the matrix material [5,48].

Effect of SIS filler Loading on Tensile Strength

Tensile strength is the maximum force at which the material can endure without fracture under stretched condition [49]. The tensile strength and tensile modulus curve of the unfilled and SIS filled NPJE composites are shown in Figure 11. It is observed that the tensile strength increases with the increased in SIS powder content in the composite from 44.24 MPa at 0 wt.% (NPJSIS-0) to 49.56 MPa at 16 wt.% (NPJSIS-2) respectively. For 16 wt.% addition of SIS powder in the composite, the tensile strength and tensile modulus is increased by 10.74 % and 6.44 % respectively. The important reason for enhancing the tensile strength is that owing to its fine and consistent delivery, the fillers adhered to the matrix very strongly. The smaller is the size of the filler particles having higher surface area, allowing the resin matrix to wet the filler [50] and hence enhancement in the strength. When the filler loading increases up to 24 wt.% (NPJSIS-3) the tensile strength is decreased by 8.27 %. The foremost reason is poor adhesion between the matrix and the fillers. Second contributing reason for reducing strength value is agglomeration of the particles, which reduces the surface area to interlock with the epoxy which causes the particles to fail in transferring the stress at fiber/matrix interface [49]. Further, the tensile modulus increases with the increased in filler wt.% in the composites because the modulus is much higher than the modulus of matrix and reinforced material, hence the modulus increases with the addition of filler particles [49]. The post tensile failure analysis is performed by scanning electron microscopy (SEM) as seen in Figure 12(a-d). Brittle fracture of the fibers and voids formation due to fiber pull out is observe in Figure 12(a) for unfilled composite NPJSIS-0. Owing to the repetitive applied tensile load the matrix fracture plane overlap and before individuating develops cleavage on both the surfaces leaving ribbon pattern as observed in the Figure 12(a). At the same time, crack initiation and propagation converges where fiber pull is less significant than elsewhere in the matrix material and similar phenomena is observed for all the composites because of the brittle nature of the epoxy [13]. Figure 12(b) show the micrographs for NPJSIS-1 and the fiber debonding, fiber pull out and debonding of the fiber and matrix can be seen. Fewer voids, good fiber, filler and matrix interfacial bonding enables the favourable stress transfer from one part to another that can be observed from Figure 12(c) which confirms the higher tensile strength of NPJSIS-2 composite as compared to the other fabricated composites. The tensile strength decreases with the higher filler wt.% due to agglomeration of the filler and fiber as indicated in Figure 12(d).

Effect of SIS filler Loading on Flexural Strength and ILSS

Flexural is the combined action of tension and compression characteristics and before yielding of the material maximum applied forced is called flexural strength. The flexural test of the fabricated composites is conducted by three-point bending test and Figure 13 shows the test results of the flexural properties of the unfilled and SIS filled NPJE composites. It is revealed from the figure that the flexural strength and flexural modulus is increased with the increase in the filler wt.% in the composite. Composite NPJSIS-3

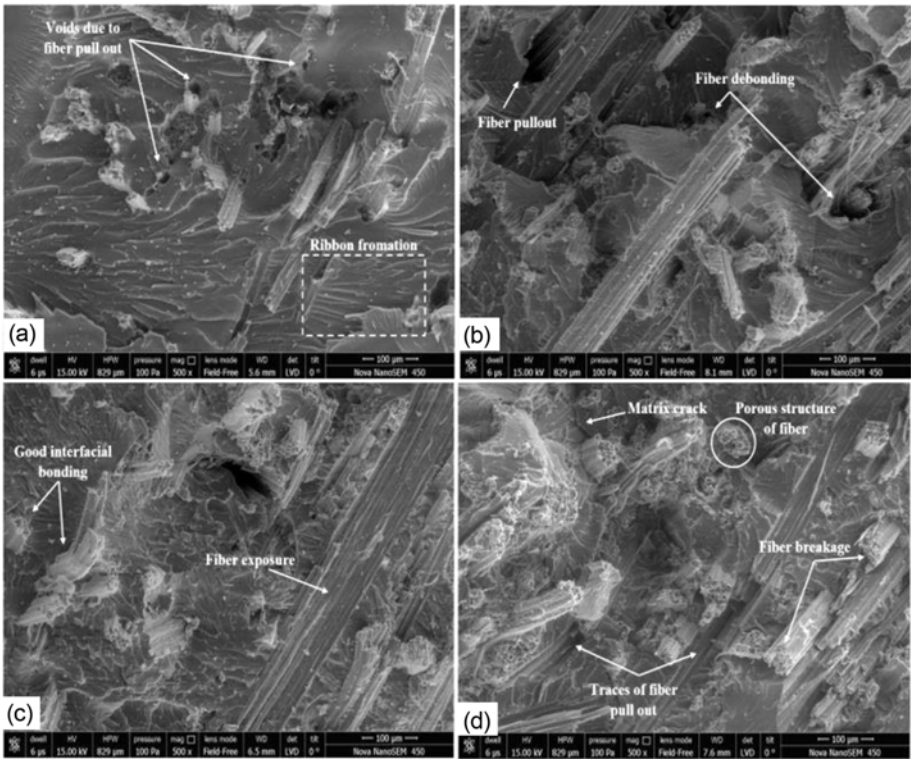

Figure 12. Micrographs of tensile tested samples (a) unfilled NPJE composite (NPJSIS-0), (b) 8 wt.% SIS filled NPJE composite (NPJSIS-1), (c) 16 wt.% SIS filled NPJE composite (NPJSIS-2), and (d) 24 wt.% SIS filled NPJE composite (NPJSIS-3).

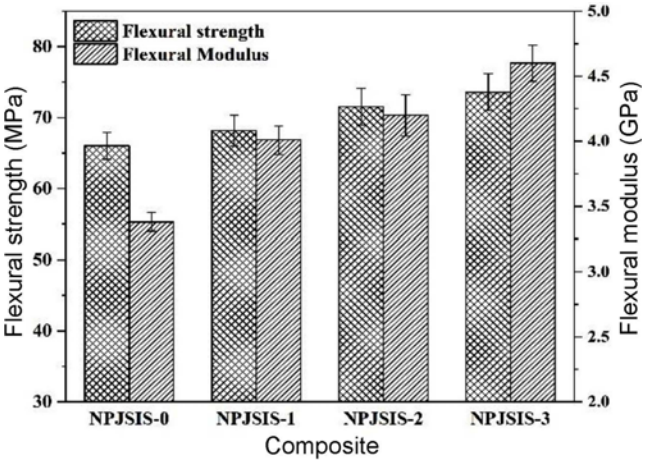

Figure 13. Flexural strength and flexural modulus of manufactured Composites.

possess maximum flexural strength and flexural modulus of 73.57 MPa and 4.6 GPa followed by NPJSIS-2 having 71.53 MPa and 4.2 GPa, NPJSIS-1having 68.16 MPa and 4.01 GPa and NPJSIS-0 having 66.01 MPa and 3.38 GPa, respectively. The increase in the flexural strength is intercalation between fiber, matrix and filler that ultimately results in good interfacial bonding, inherent toughening mechanism due to inclusion of fillers [50] and the good dispersion of the filler in the composite [14]. The flexural modulus of NPJSIS-3 is improved by ~26 % compared to NPJSIS-0 (Figure 13) which shows the modulus is dependent on the filler loading [49] and is in good agreement with the available literature [13,23]. The flexural failure generally takes place under tension- compression mode, Figure 14(a-d) shows the micrographs of the flexural tested samples of unfilled and SIS filled NPJE epoxy composites. Figure 14(a) depicts the microstructure of the unfilled NPJSIS-0 composite and fiber pull out, matrix cracking and fiber/matrix debonding is observed. The maximum flexural strength is observed for NPJSIS-3 along with the proper distribution of filler, good interfacial bonding as observed in Figure 14(d). NPJISIS-1 and NPJSIS-2 acquired an intermediate flexural strength, voids due to fiber pull out, matrix failure, and crack propagation as illustrated in Figure 14(b and c). The voids formed due to entrapped air during the composite fabrication procedure can also be witnessed in Figure 14(b).

The ILSS defines the shear strength between the composite layers, which is calculated using Short-Beam Shear (SBS) method. The effect of filler loading on ILSS is shown in Figure 15 and observed that the trend is similar to flexural strength. It is observed from the figure that the ILSS increase from 7.42 MPa to 10.09 MPa with the increased in the filler wt.% from 0 to 24 wt.%. The enhancement of ILSS

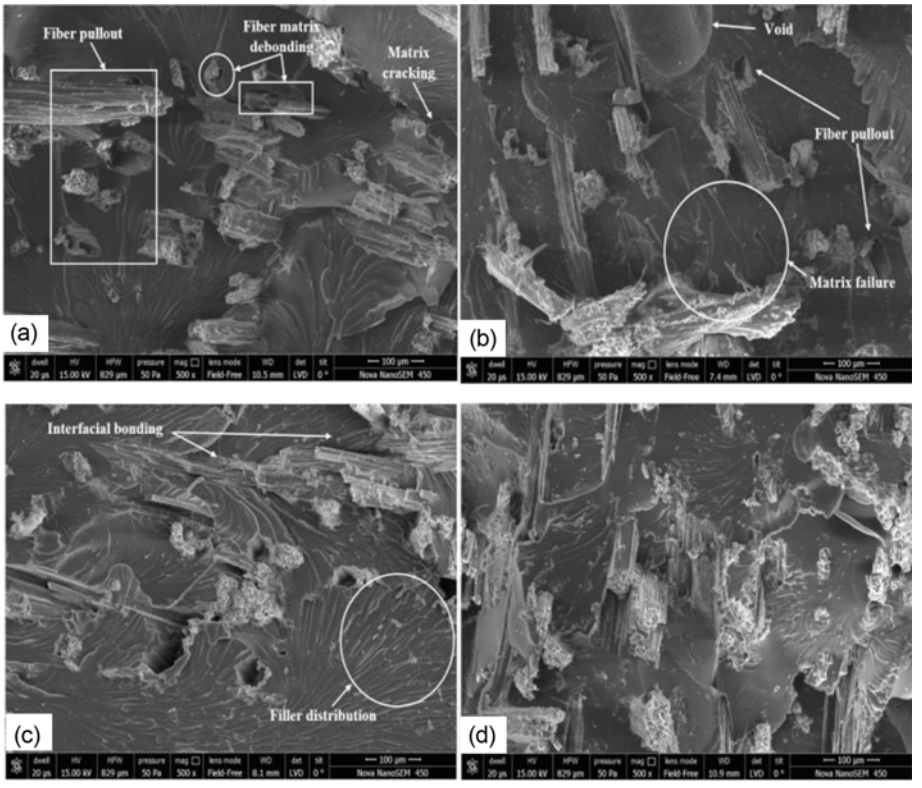

Figure 14. Micrographs of flexural tested samples (a) unfilled NPJE composite (NPJSIS-0), (b) 8 wt.% SIS filled NPJE composite (NPJSIS-1), (c) 16 wt.% SIS filled NPJE composite (NPJSIS-2), and (d) 24 wt.% SIS filled NPJE composite (NPJSIS-3).

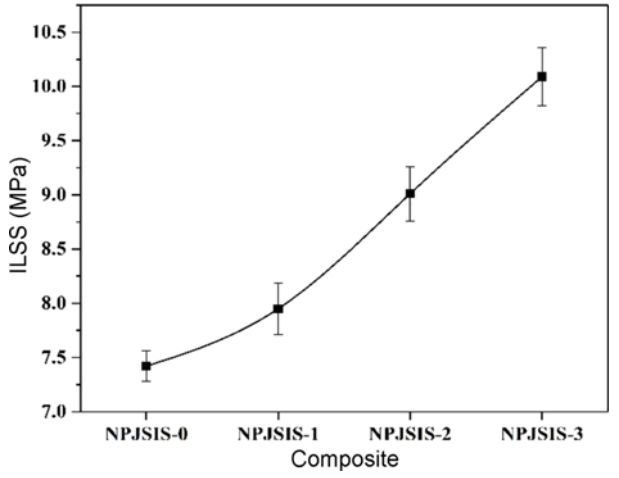

Figure 15. ILSS of manufactured composites.

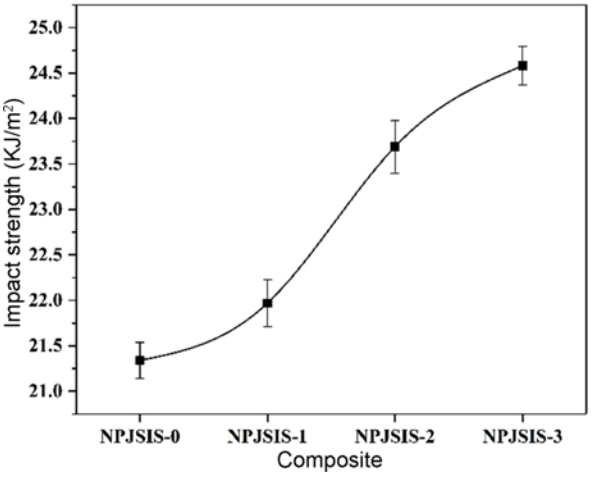

Figure 16. Impact strength of manufactured composites.

upto ~26 % is attributed to the proper distribution and compaction of filler between the fiber layers that increases the mechanical interlocking during shearing consequently resulting in the improved ILSS of the composites [14]. In addition, the filler acts as a barrier to pass shear stress from one part to another. Similar, observation has been reported by Sharma and Patnaik [13] in their previous work and Choudhary *et al*. [14] for marble dust filled composites.

Effect of SIS filler Loading on Impact Strength

Composite impact strength is largely influenced by the stiffness, complexity of the interface field and fiber separation from the matrix creates friction work. The impact strength of the composite shows a proportional relation with the filler

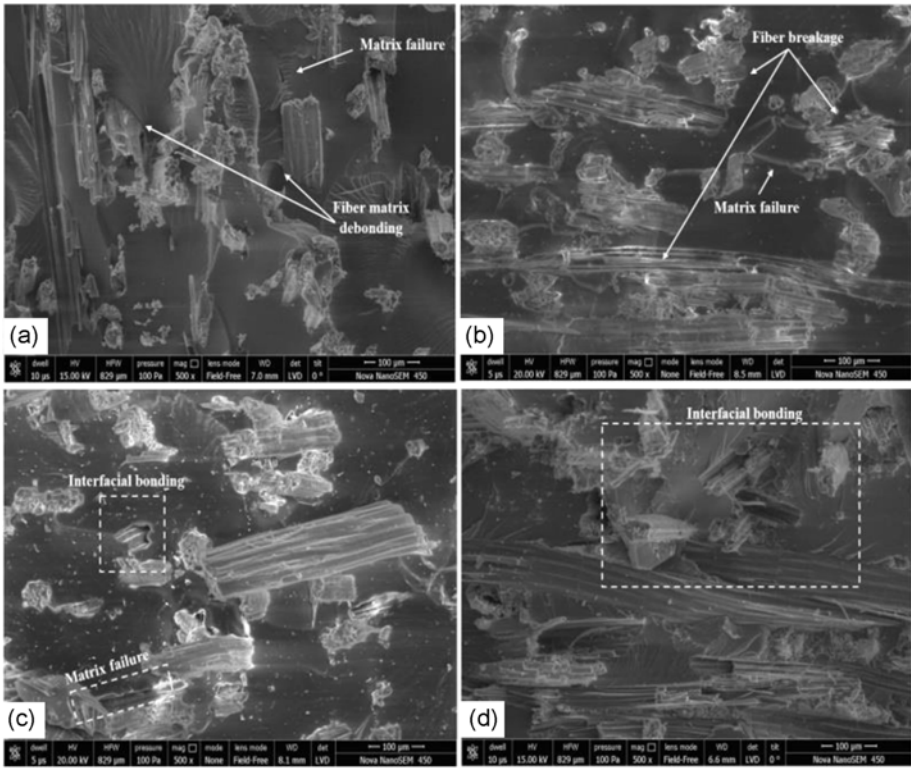

Figure 17. Micrographs of impact tested samples (a) unfilled NPJE composite (NPJSIS-0), (b) 8 wt.% SIS filled NPJE composite (NPJSIS-1), (c) 16 wt.% SIS filled NPJE composite (NPJSIS-2), and (d) 24 wt.% SIS filled NPJE composite (NPJSIS-3).

loading as observed from the Figure 16. The impact strength of unfilled composite NPJSIS-0 is observed as 21.34 KJ/mm^2 and further increases to 21.97 KJ/mm^2, 23.69 KJ/mm^2 and 24.58 KJ/mm^2 with the increasing SIS wt.% from 8 to 24 wt.% in the composite, respectively. It can be revealed from the figure that the inclusion of SIS powder as a filler in the composite gives better impact resistance compared to unfilled NPJE composite which is attributed to that energy absorbed during impact test by the SIS particles in the plane of fracture resulting resistance of the fracture failure growth [23]. The improvement is also attributed to the adhesion with jute and SIS powder in the composite [51]. Similarly, Patnaik and Nayak [23] studied the effect of silicon carbide filled jute epoxy composite on the mechanical properties. The impact strength was increased from 55 J to 63 J with the increased in the wt.% of filler from 0 to 15 wt.%. Pawar *et al*. [39] also found the improvement in the impact strength with the increase in wt.% of granite powder from 8 to 24 wt.% in the jute fiber reinforced composite. Composite NPJSIS-0 possess lowest impact strength whereas NPJSIS-1 and NPJSIS-2 shows the intermediate impact strength due to smaller wt.% of filler, matrix failure, fiber breakage and interfacial bonding between fiber and matrix which can be observed from the micrographs shown in Figure 17(a, b and c) also good interfacial bonding can be observed for NPJSIS-3 in Figure 17(d).

Effect of SIS filler Loading on Compressive Strength

The compressive strength is the resistance of the material to fail under compression loading and compressive strength as a function of filler loading is shown in Figure 18. It is observed from the figure that the compressive strength increases with the increased in the SIS wt.% in the composite. The compressive strength of the NPJSIS-0, NPJSIS-1, NPJSIS-2 and NPJSIS-3 is found 56.22 MPa, 60.72 MPa,

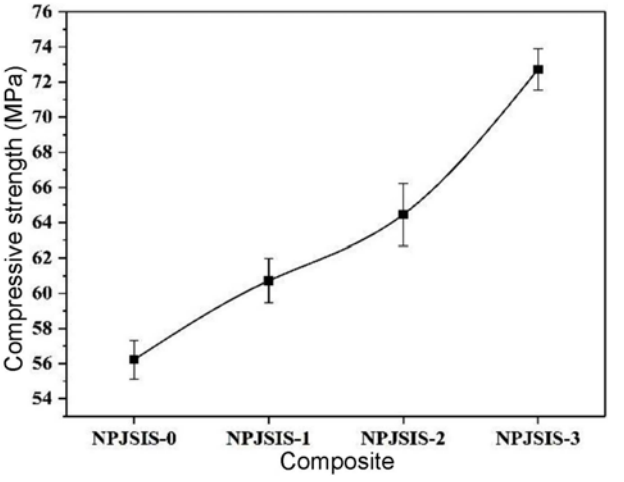

Figure 18. Compressive strength of manufactured composites.

64.46 MPa and 72.72 MPa, respectively. It has been seen that the improvement in the compressive strength by ~23 % with addition of 24 wt.% of SIS powder. In compression the failure is primarily due to micro buckling of fiber and shear crippling and the inclusion of filler in the composite acts as a resistance to the buckling, causing increase in the compressive strength with the increased in the SIS weight percentage in the composite from 0 to 24 wt.%. In the present study, the specimens are mostly failed under shear-compression failure mode, in which the fiber and matrix interface may fracture under shear due to buckling of fiber under compression load and failure of the specimen takes place [3].

Effect of SIS filler Loading on Fracture Toughness

Fracture toughness is the property of material indicating the resistance to the fracture. Figure 19 shows the fracture toughness in terms of critical stress intensity factor of unfilled and SIS powder filler NPJE composites. It is evident from the figure that the K_{Ic} increased with the increasing wt.% of SIS powder loading from 0 to 24 wt.% in the composite. The K_{Ic} values for the NPJSIS-0, NPJSIS-1, NPJSIS-2, and NPJSIS-3 are 2.63 MPa·$m^{1/2}$, 3.19 MPa·$m^{1/2}$, 3.29 MPa·$m^{1/2}$ and 3.64 MPa·$m^{1/2}$, respectively. It is observed that the NPSIS-3 exhibits maximum value of fracture toughness and the improvement is recorded of ~28 % compared to unfilled composite (NPJSIS-0). The obtained results are in the line with the previously reported studies by Pawar *et al*. [39] and Choudhary *et al*. [14] where increasing the filler loading increased the fracture toughness. The enhancement in the fracture toughness with the filler loading in the composite is attributed to the crack pinning, in which filler particles absorbs the energy and invents obstruction in the propagation path of crack front [12]. Additionally, at tip the crack driving force is divided into several direction via crack twisting which leads to reduce the crack propagation intensity and hence the fracture toughness increases [14]. Crack tip blunting may also be the reason for the improvement of the fracture toughness with filler loading, where the crack propagation time is delayed due to debonding of the filler and specimen sustaining larger load [52].

Effect of SIS filler Loading on Thermal Conductivity

The experimental thermal conductivity of the unfilled and SIS powder filled composites is depicted in Figure 20. The experimental obtained values for thermal conductivity of NPJSIS-0, NPJSIS-1, NPJSIS-2 and NPJSIS-3 are 0.2115 W/m-K, 0.2817 W/m-K, 0.3015 W/m-K and 0.3172 W/m-K, respectively. It can be clearly observed from the figure that the thermal conductivity of the composite increases with the increased in the filler loading from 0 to 24 wt.% in the composite. The enhancement in the thermal conductivity is attributed to the fact that the filler particles in the composite acts as a heat carrier and as the filler wt.% increases the continuous thermal path may be formed. Also, the experimental values of the thermal conductivity for the developed composites are compared with the computed values established via theoretical models viz. series model, parallel model, GMM and B & M model. In the case of low volume fraction of filler, a number of filler particles are not adequate to constitute a conductive chain through the thickness and hence has a minimum effect of filler-fiber-matrix property and is closer to the series model. However, as the number of filler particles are increased due to the higher volume fraction, it enables to form a continuous conductive chain which helps in elevating the thermal conductivity of the composites and hence near to the parallel model [19,30,53].

The order of the bound of effective thermal conductivity is parallel model > FEA model ≈ experimental > B & M model > GMM > series model as observed from Figure 20. It can be seen that the values obtained from FEA models is in the good agreement with the experimental values. Hence, finite

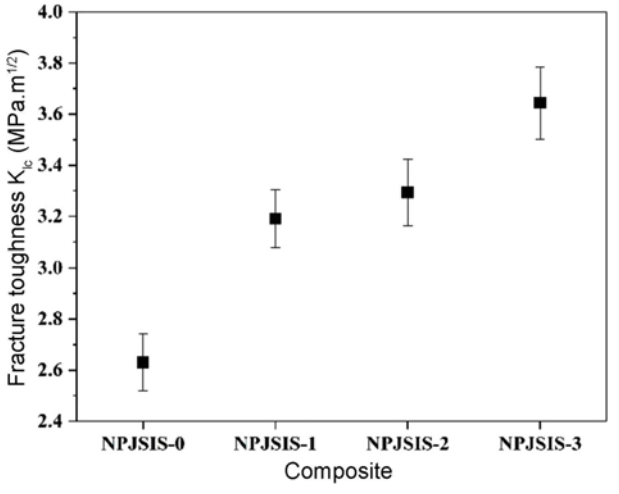

Figure 19. Fracture properties of manufactured composites.

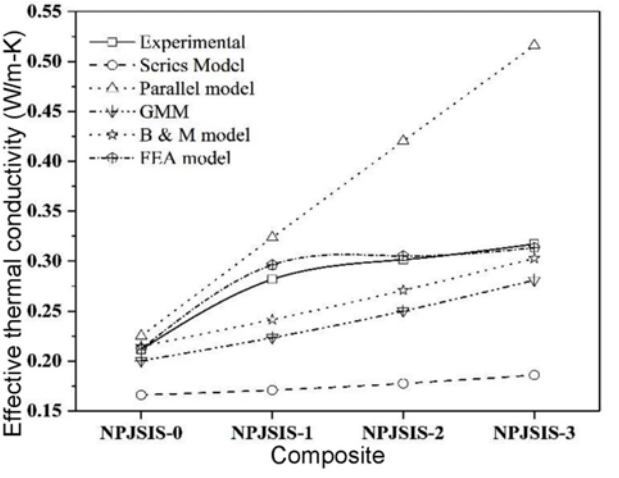

Figure 20. Comparison of thermal conductivities estimated from different models for manufactured composites.

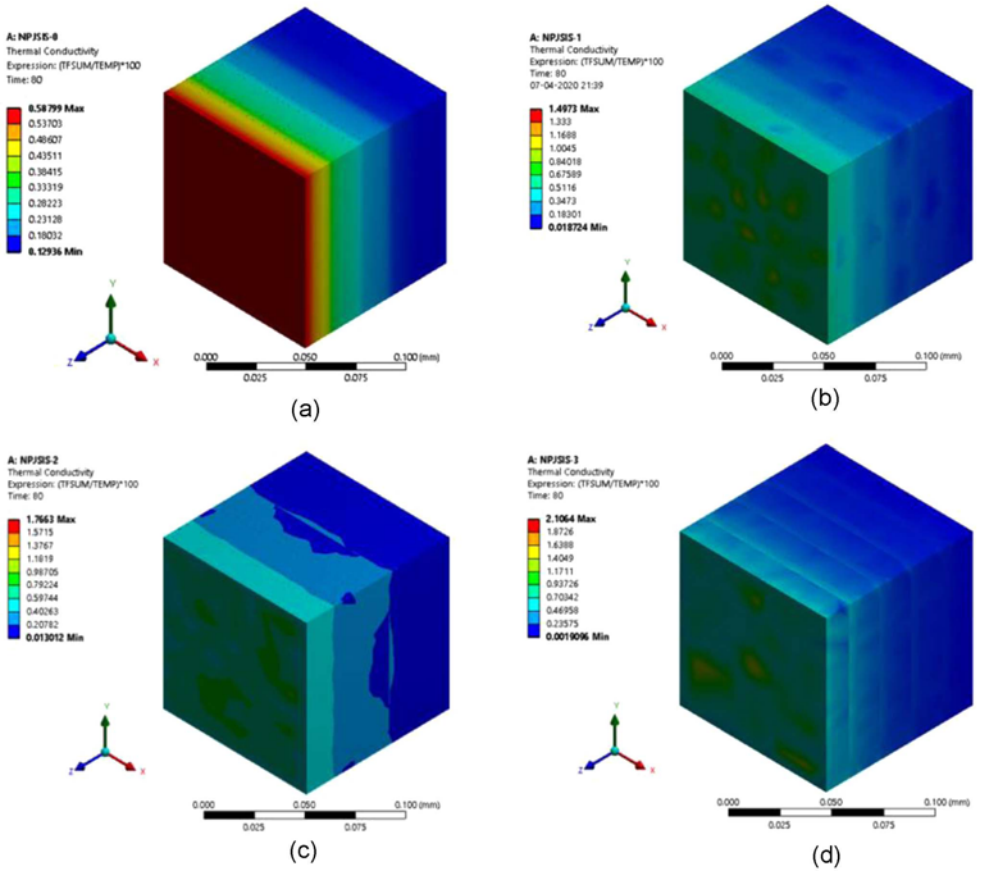

Figure 21. Thermal conductivity profile for (a) unfilled NPJE composite (NPJSIS-0), (b) 8 wt.% SIS filled NPJE composite (NPJSIS-1), (c) 16 wt.% SIS filled NPJE composite (NPJSIS-2), and (d) 24 wt.% SIS filled NPJE composite (NPJSIS-3).

element simulation can be very well used to predict the effective thermal conductivity for a wide range of filler loading in three phase composites for this type. Figure 21 shows the thermal conductivity pattern for unfilled and SIS filled from 8 wt.% to 24 wt.% NPJE composites. The heat conduction across the SIS filled composite occurs mainly through fillers compared to unfilled composite and at NPJSIS-1, most of the SIS particulates are not in the contact due to which weak thermal chain is formed and hence lower thermal conductivity is observed compared to NPJSIS-2 and NPJSIS-3.

Dynamic Mechanical Analysis (DMA)

The findings on the storage modulus (E') help to evaluate the elastic properties of the hybrid composite in three regions such as glass (room temperature to 47 °C), transition (47 °C to 84 °C) and rubbery region (above 84 °C) [15]. Figure 22 shows the variation in storage modulus with temperature (25 ° to 180 °C) for SIS filled and unfilled needle NPJE composites. The E' of 8, 16 and 24 wt.% filled SIS composite at room-temperature improved compared with the unfilled jute epoxy composite. This may be due to great stress transfer at the interface of fiber and matrix [54]. At low temperature, E' of NPJSIS-1, NPJSIS-2, NPJSIS-3

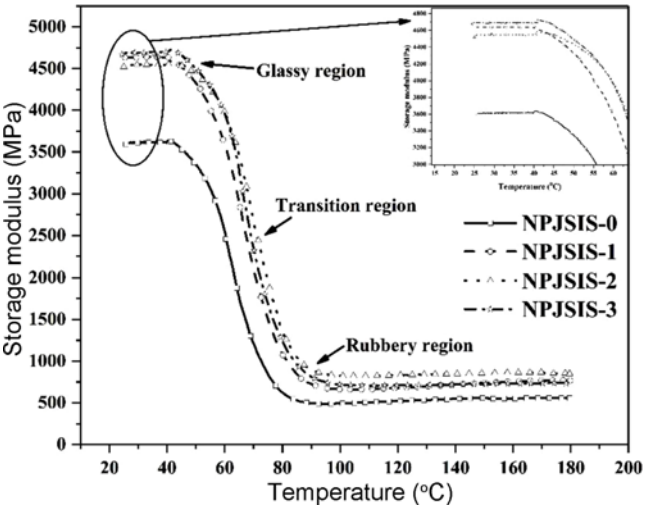

Figure 22. Storage modulus vs. temperature of manufactured composites.

are observed to be close to each other with the highest E' values 4636.87 MPa, 4550.30 MPa and 4693.48 MPa respectively. This emphasizes that at low-temperatures fillers are not contributing much to communicate the stiffness of the composites. It is observed from the figure that in glassy region (region I) the molecules are compact and further increase in the temperature the molecules slightly loses their strength resulting in the decrease in the storage modulus and stiffness of the composites [55]. Further with the increased in the temperature from 47 °C to 84 °C (transition region) the E' of the composites significantly declines, which is attributed to the softening of the matrix at the glass transition region. Above glass transition temperature the NPJSIS-2 curve shows better E' value compared to NPJSIS-1 and NPJSIS-3 which attributes that the addition of SIS up to 20 % limits the movement of polymer chain as they embed in the fiber and matrix [56]. In the rubbery region it is found that NPJSIS-2 possesses highest value of E' and this fact shows that the composite with 16 wt.% filler shows better adhesion and interface bonding compared to composites with 8 wt.% and 25 wt.% of SIS powder as filler [57]. It is also seen from the fig that after 84 °C (Region III) the modulus is unaffected by the temperature and remained constant. Nevertheless, when the temperature increases the composite constituents tend to show increased molecular mobility and thus lose their tight packing structure and then progressively decreases the modulus in the rubbery region [58]. It is revealed from the figure that the inclusion of SIS in the NPJE composites enhanced the storage modulus. The order of the magnitude of E' at lower temperature specifically between 20 °C to 40 °C is NPJSIS-3 > NPJSIS-1 > NPJSIS-2 > NPJSIS-0.

Loss modulus is a viscous response the materials regarded as the amount of heat dissipated by the samples under stress as heat/cycle [56,58]. The loss modulus (E") versus temperature curve for unfilled and SIS filled NPJE composite at 1 Hz frequency is shown in Figure 23. Similar to storage modulus, loss modulus curve is also showing improvement in E" with the inclusion of the filler particles in the composite from 0 to 24 wt.%. It is observed from the figure that all loss modulus curves reached to the optimal values for maximum dissipation of energy and decreased with the further increase in the temperature, which is attributed to the free movement of polymer chain. Figure 23 shows the lower peak for unfilled NPJE composite but inclusion of SIS filler into the composite increases the loss modulus peak values. Interestingly, similar to E', the higher E" peak height is observed for NPJSIS-2 with 496.14 MPa compared with NPJSIS-1 (peak height 378.74), NPJSIS-3 (peak height 377.97) and NPJSIS-0 (peak height 330.75) which is attributed to proper distribution of the filler, dispersion and no agglomeration of the filler in the composite [59]. Also, the addition of filler in the composite acts as a blockade in the movement of matrix molecules and higher thermal

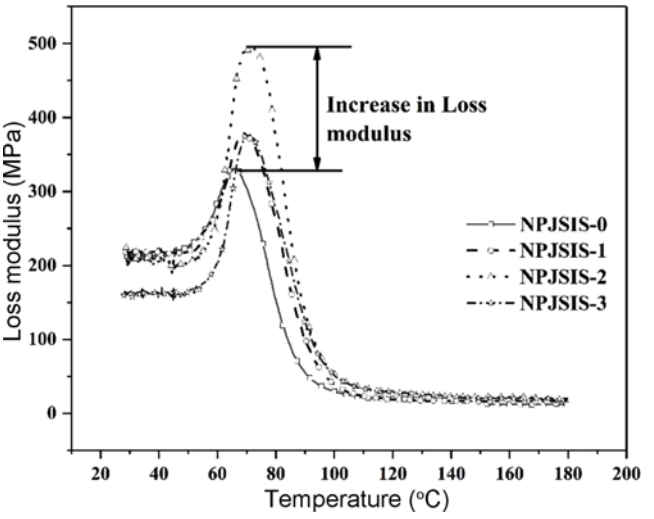

Figure 23. Loss modulus vs. temperature of manufactured composites.

stability is associated in enhancing the E" of the composite [54]. In rubbery region (beyond 95 °C), the liner curves with the negligible decrease in the loss modulus is observed with the further increase in the temperature. The findings of the current research study are partly consistent with the observations made by Choudhary *et al*. [54] and Pawar *et al*. [15] respectively.

The damping factor (Tan δ) is the ratio of loss and storage modulus, is a measure of impact and elastic characteristics of a material, the peak height is related to the energy dissipation and impact properties of a material which means higher the peak would result in better impact properties and less internal energy dissipation [58,59]. The major involvement to the composite damping is due to the nature of the reinforce and matrix material, nature of interphase, frictional damping due to slip in the unbound regions between fiber and matrix interface and damping due to energy dissipation in the area of the matrix cracks and broken fibers [60]. The glass transition temperature (T_g) of the composite can also be estimated from the temperature corresponding to the Tan δ peak. The Tan δ of the unfilled and SIS filled NPJE composites as a function of temperature are shown in Figure 24. It is observed from the figure that the glass transition temperature (T_g) i.e. peak of Tan δ curve of the unfilled and SIS filled NPJE composites is 75.1 °C, 79.6 °C, 79.3 °C and 80.9 °C respectively, as presented in Table 3. It can be concluded that the inclusion of SIS powder in the composite caused the peak of Tan δ to shift towards the higher temperature which is attributed to the fact that addition of the filler in the composite increases the brittleness which causes restrictions in the movement of the epoxy molecules [54]. It is also revealed from the Figure 24 that the NPJSIS-0 possess highest peak (0.2836) showing higher degree of movement of molecules [59]. Addition of SIS powder in the

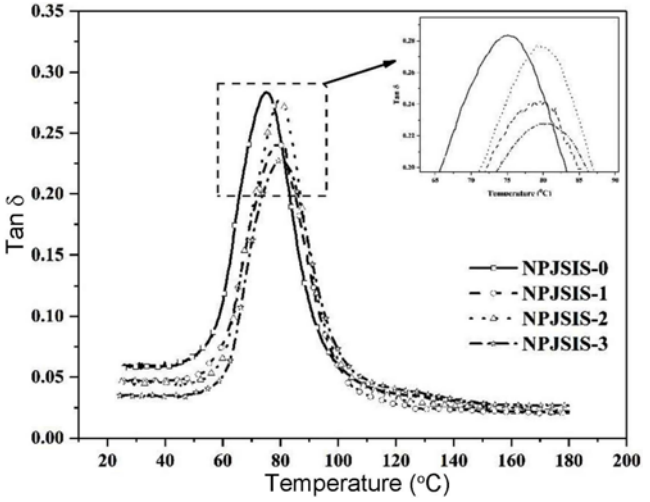

Figure 24. Damping factor vs. temperature of manufactured composites.

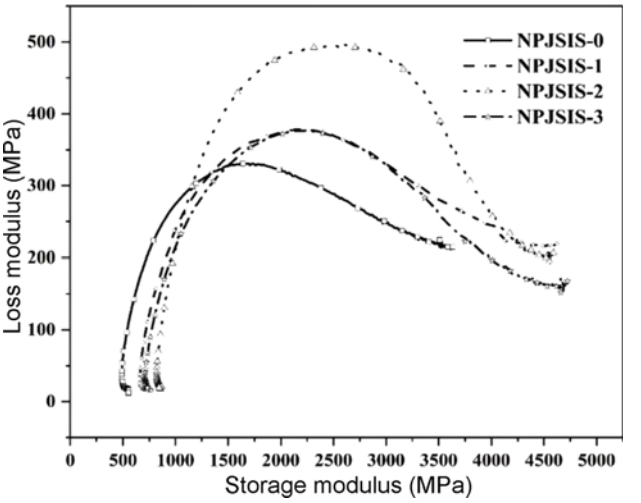

Figure 25. Cole-Cole plot for manufactured composites.

Table 3. Peak height and glass transition temperature from DMA

Composite	Loss modulus (MPa) E''_{max}	Damping factor (Tan δ_{max})	Glass transition temperature (°C)	
			E''_{max}	Tan δ_{max}
NPJSIS-0	330.75	0.2836	65.9	75.1
NPJSIS-1	378.74	0.2424	69.1	79.6
NPJSIS-2	496.14	0.2766	70.3	79.3
NPJSIS-3	377.97	0.2281	70.47	80.9

composite shows comparatively lower peak height and NPJSIS-3 shows lowest value of Tan δ peak height (0.2281). The incorporation of SIS particles in the composite creates the barrier for the movement of epoxy molecules, slow down the internal energy dissipation process and hence reduces the damping factor [54,59].

Cole-Cole plot is the graphical representation to interpret the relationship between E" with E' and illustrated in Figure 25. Past researchers claimed that homogenous and properly dispersed filler in the composite exhibits smooth semi-circular curve whereas, irregular shape of semi-circular arc signifies only heterogeneous in nature of the composites [54,59]. It is observed from the figure that the unfilled and SIS powder filled composites exhibits imperfect semicircle curve which shows the heterogeneous nature of the material [60]. It can be observed from the figure that NPJSIS-1 and NPJSIS-3 curve are found to be less heterogeneous in nature as compared to unfilled NPJE composite which is attributed that the incorporation of filler in the composite helps to overcome the heterogeneity nature in the composite. However, the shape of the curves is representing the good fiber-matrix bonding [60]. Similar, observation was made by Chaudhary *et al*. [54] for marble dust filled glass fiber reinforced polymer composites.

Conclusion

In this research work, NPJE composite with varying sponge iron slag weight percentage from 0 to 24 wt.% is fabricated using VARTM and characterized to study their physical, mechanical, thermal and thermomechanical properties respectively. ANSYS simulation has been carried out to predict the effective thermal conductivities of the composites. The water absorption percentage for all these composites increases with the increased in immersion time and attains a saturation state at 7.02 % for NPJSIS-3. The diffusion coefficient for NPJSIS-0 and NPJSIS-1 is observed to be 10.38×10^{-5} mm^2/s and 20.88 mm^2/s respectively, but further increased in wt.% of SIS powder causes the diffusivity of the composites decrease and found that the diffusion coefficient for NPJSIS-2 and NPJSIS-3 is decreased by 7.65 % and 7.76 % compared with NPJSIS-1 which shows good bonding between fiber, matrix and filler in the composites. The tensile strength of the fabricated composite shows increasing in trend up to 16 wt.% filler content whereas, the tensile modulus tends to increase with the increased in the filler wt.% in the composite. Flexural strength, ILSS, impact strength and compressive strength show increasing in trend with the filler wt.% in the composites. The improvement in the flexural strength is observed as 10.28 % whereas, the flexural modulus and ILSS are enhanced by ≈ 26 % with inclusion of SIS powder in the composite. The improvement in impact and compressive strength are observed by 13.18 % and 23 %, respectively. The fracture toughness is also enhanced with filler loading in the composites and the maximum value of fracture toughness is observed for NPJSIS-3 with 3.64 $MPa\cdot m^{1/2}$. The possible failure mechanism concerned with the fracture are fiber pull out, matrix failure,

crack pining and crack tip blunting for unfilled and SIS filled composites. Improvement in the thermal conductivities are observed with filler wt.%. The orders of experimental thermal conductivities are NPJSIS-3 > NPJSIS-2 > NPJSIS-1 > NPJSIS-0. ANSYS as a significant tool to predict the thermal conductivity of the developed composites. The FEM approach is used to assess the thermal conductivity of these materials with a varying in filler loading. The values of the thermal conductivities obtained for finite element analysis are in the good agreement with the experimental values. The order of the bound of effective thermal conductivity is parallel model > FEA model ≈ experimental > B & M model > GMM > series model. The addition of SIS powder in the NPJE composites enhanced the storage modulus of the composite and ≈ 30 % enhancement is observed for NPJSIS-3 compared to NPJSIS-0 at 30 °C and heterogeneity of the developed composites are presented by Cole-Cole plot.

In the present study the jute fiber is considered as a reinforced material, since it is biodegradable, non-toxic, eco-friendly, easily available and low cost material compared to other available synthetic fibers, the developed composite may be suitable for multiple number of applications such as roofing, partition wall, automobile parts and it may be a good replacement of wood for interior as well exterior applications.

Acknowledgment

The authors acknowledge the TEQIP-III, MNIT Jaipur for financial support, Advanced research lab for Tribology, Materials Research Center (MRC), MNIT, Jaipur, India and Vincenzo Solutions Private Limited, Jaipur, India for fabrication and testing facilities.

References

1. R. Mishra, J. Wiener, J. Militky, M. Petru, B. Tomkova, and J. Novotna, *Fiber. Polym.,* **21**, 619 (2020).
2. T. Singh, P. Pattnaik, C. I. Pruncu, A. Tiwari, and G. Fekete, *Polym. Test.,* **89**, 106614 (2020).
3. T. Singh, C. I. Pruncu, B. Gangil, V. Singh, and G. Fekete, *J. Mater. Res. Technol.,* **9**, 1491 (2020).
4. L. Gardner, T. Munro, E. Villarreal, K. Harris, T. Fronk, and H. Ban, *Fiber. Polym.,* **19**, 393 (2018).
5. M. Gupta and R. Srivastava, *Indian J. Fibre Text. Res.,* **42**, 64 (2017).
6. M. K. Gupta, *J. Mater. Environ. Sci.,* **9**, 100 (2018).
7. V. Chaudhary, P. K. Bajpai, and S. Maheshwari, *J. Nat. Fibers.,* **15**, 80 (2018).
8. T. Singh, B. Gangil, B. Singh, S. K. Verma, D. Biswas, and G. Fekete, *J. Mater. Res. Technol.,* **8**, 5961 (2019).
9. W. Zhen-yu, W. Jie, C. Feng-hong, M. Yun-hai, T. Singh, and G. Fekete, *Mater. Res. Express.,* **6**, 075103 (2019).
10. X. Y. Liu and G. C. Dai, *Express Polym. Lett.,* **1**, 299 (2007).
11. N. Karabulut, M. Aktaş, and H. E. Balcıoğlu, *J. Nat. Fibers,* **16**, 629 (2019).
12. R. Kumar, K. Kumar, S. Bhowmik, and G. Sarkhel, *J. Polym. Res.,* **26**, 54 (2019).
13. A. Sharma and A. Patnaik, *JOM-J. Min. Met. Mat. S*, **70**, 1284 (2018).
14. M. Choudhary, T. Singh, A. Sharma, M. Dwivedi, and A. Patnaik, *Mater. Res. Express.,* **6**, 105702 (2019).
15. M. J. Pawar, A. Patnaik, and R. Nagar, *Polym. Compos.,* **38**, 736 (2017).
16. S. K. Verma, A. Gupta, T. Singh, B. Gangil, E. Jánosi, and G. Fekete, *Mater. Res. Express.,* **6**, 125704 (2019).
17. A. Gupta, A. Kumar, A. Patnaik, and S. Biswas, *J. Surf. Eng. Mater. Adv. Technol.,* **2**, 149 (2012).
18. P. K. Patnaik and S. Biswas, *Adv. Polym. Technol.,* **37**, 1764 (2018).
19. R. Kaundal, A. Patnaik, and A. Satapathy, *Silicon,* **4**, 175 (2012).
20. P. K. Patnaik, P. T. R. Swain, and S. Biswas, *Polym. Compos.*, **40**, 2335 (2019).
21. M. H. Rafiquzzaman, A. Rahman, M. Sayeed, A. Nawazish, and M. H. Rahman, *Int. J. Mech. Eng. Autom.,* **03**, 202 (2016).
22. A. Shalwan and B. F. Yousif, *Mater. Des.,* **59**, 264 (2014).
23. T. K. Patnaik and S. S. Nayak, *Silicon,* **10**, 137 (2018).
24. S. N. Leung, M. O. Khan, E. Chan, H. Naguib, F. Dawson, V. Adinkrah, and L. Lakatos-Hayward, *Compos. Part B Eng.,* **45**, 43 (2013).
25. A. Patnaik, M. Abdulla, A. Satapathy, S. Biswas, and B. K. Satapathy, *Mater. Des.,* **31**, 837 (2010).
26. D. Kumlutas and I. H. Tavman, *J. Thermoplast. Compos. Mater.,* **19**, 441 (2006).
27. A. D. Brailsford and K. G. Major, *Br. J. Appl. Phys.,* **15**, 313 (1964).
28. G. Buonanno and A. Carotenuto, *Int. J. Heat Mass Transf.,* **40**, 393 (1997).
29. A. Moosavi and P. Sarkomaa, *J. Phys. D. Appl. Phys.,* **36**, 1644 (2003).
30. A. Patnaik, P. Kumar, S. Biswas, and M. Kumar, *Comput. Mater. Sci.,* **62**, 142 (2012).
31. B. Z. Gao, J. Z. Xu, J. J. Peng, F. Y. Kang, H. D. Du, J. Li, S. W. Chiang, C. J. Xu, N. Hu, and X. S. Ning, *Thermochim. Acta,* **614**, 1 (2015).
32. A. Sharma, V. R. Kiragi, M. Choudhary, S. K. Biswas, and A. Patnaik, *Mater. Res. Express.,* **6**, 105318 (2019).
33. A. Sharma, A. Purohit, R. Nagar, and A. Patnaik, *SSRN Electron. J.,* https://doi.org/10.2139/ssrn.3322501 (2019).
34. M. Choudhary, A. Sharma, M. Dwivedi, and A. Patnaik, *Fiber. Polym.,* **20**, 823 (2019).
35. S. Kumar, V. K. Patel, K. K. S. Mer, B. Gangil, T. Singh, and G. Fekete, *J. Nat. Fibers.,* https://doi.org/10.1080/15440478.2019.1612814 (2019).
36. A. M. Thiele, A. Kumar, G. Sant, and L. Pilon, *Int. J. Heat Mass Transf.,* **73**, 177 (2014).
37. R. D. Sweeting and X. L. Liu, *Compos. Part A Appl. Sci.*

Manuf., **35**, 933 (2004).
38. R. Nayak, D. P. Tarkes, and A. Satapathy, *Comput. Mater. Sci.,* **48**, 576 (2010).
39. M. J. Pawar, A. Patnaik, and R. Nagar, *Polym. Compos.,* **38**, 1335 (2017).
40. M. R. Kulkarni and R. P. Brady, *Compos. Sci. Technol.,* **57**, 277(1997).
41. Z. Li, H. Chen, L. Cai, Z. Zhu, Y. Wang, and Y. Zhang, *J. Reinf. Plast. Compos.,* **31**, 1586 (2012).
42. Q. Liu and P. Ming, *Heat Transf. Part B Fundam.,* **73**, 363 (2018).
43. L. Tan, X. Shi, T. Cheng, X. Zeng, and H. Zheng, *Appl. Therm. Eng.,* **160**, 113949 (2019).
44. F. Wang, L. T. Drzal, Y. Qin, and Z. Huang, *J. Mater. Sci.,* **51**, 3337 (2016).
45. A. Satapathy, A. Kumar Jha, S. Mantry, S. K. Singh, and A. Patnaik, *J. Reinf. Plast. Compos.,* **29**, 2869 (2010).
46. S. K. Saw, K. Akhtar, N. Yadav, and A. K. Singh, *J. Nat. Fibers,* **11**, 39 (2014).
47. R. K. Nayak and B. C. Ray, *Arch. Civ. Mech. Eng.,* **18**, 1597 (2018).
48. R. K. Nayak, K. K. Mahato, and B. C. Ray, *Compos. Part A.,* **90**, 736 (2016).
49. S. Y. Fu, X. Q. Feng, B. Lauke, and Y. W. Mai, *Compos. Part B Eng.,* **39**, 933 (2008).
50. A. Vinod, R. Vijay, and D. L. Singaravelu, *J. Nat. Fibers,* **15**, 648 (2018).
51. T. Alomayri, F. U. A. Shaikh, and I. M. Low, *Compos. Part B Eng.,* **60**, 36 (2014).
52. K. J. Wong, B. F. Yousif, K. O. Low, Y. Ng, and S. L. Tan, *J. Strain Anal. Eng. Des.,* **45**, 67 (2010).
53. R. Nayak, D. P. Tarkes, and A. Satapathy, *Comput. Mater. Sci.,* **48**, 576 (2010).
54. M. Choudhary, T. Singh, M. Dwivedi, and A. Patnaik, *Polym. Compos.,* **40**, 4113 (2019).
55. J. M. Ferreira, C. Capela, J. Manaia, and J. D. Costa, *Mater. Res.,* **19**, 702 (2016).
56. N. Saba, M. Jawaid, O. Y. Alothman, and M. T. Paridah, *Constr. Build. Mater.,* **106**, 149 (2016).
57. S. Keusch and R. Haessler, *Compos. Part A Appl. Sci. Manuf.,* **30**, 997 (1999).
58. S. Shinoj, R. Visvanathan, S. Panigrahi, and N. Varadharaju, *Biosyst. Eng.,* **109**, 99 (2011).
59. N. Saba, A. Safwan, M. L. Sanyang, F. Mohammad, M. Pervaiz, M. Jawaid, O. Y. Alothman, and M. Sain, *Int. J. Biol. Macromol.,* **102**, 822 (2017).
60. L. A. Pothan, Z. Oommen, and S. Thomas, *Compos. Sci. Technol.,* **63**, 283 (2003).